https://doi.org/10.5194/egusphere-2024-2977
Preprint. Discussion started: 29 October 2024

Real-time Monitoring and Analysis of Debris Flow Events: Insight from seismic signal characteristics

Yan Yan[a,c], Cheng Zeng[a] , Renhe Wang[a], Yifei Cui[b]*, Sheng Hu[d], Xinglu Wang[a], Hui Tang[e]

[a] Key Laboratory of High-Speed Railway Engineering, MOE/School of Civil Engineering, Southwest Jiaotong University, Chengdu 610031, China

[b] State Key Laboratory of Hydroscience and Engineering, Tsinghua University, Beijing 100084, China

[c] Section 4.6: Geomorphology, German Research Centre for Geosciences (GFZ), Potsdam 14473, Germany

[d] College of Urban and Environmental Sciences, Northwest University, Xi'an 710127, China

[e] Section 4.7: Earth Surface Process Modelling, German Research Centre for Geosciences (GFZ), Potsdam 14473, Germany

*Corresponding author: Yifei Cui, e-mail: yifeicui@mail.tsinghua.edu.cn

https://doi.org/10.5194/egusphere-2024-2977
Preprint. Discussion started: 29 October 2024

Abstract

Debris flows triggered by rainfall are among the world's most dangerous natural hazards due to their abrupt onset, rapid movement, and large boulder loads that can cause significant loss of life and infrastructure. Monitoring and early warning are key strategies for mitigating debris flows. However, deploying large instruments for continuous monitoring in challenging terrains like Wenchuan, China, is difficult due to complex topography and limited access to electricity and batteries. Recognizing the effectiveness of environmental seismology in monitoring geohazards, our study aims to establish a cost-effective, reliable, and practical debris flow monitoring system based on seismic monitoring in Wenchuan, China. We analyzed seismic signals and infrared images to determine debris flow characteristics and behavior. Through a case study in Fotangba Gully, we demonstrated how seismic signals can be used to track debris flow duration and confirm rainfall as the trigger. Using the cross-correlation function, we calculated the maximum velocity of the debris flow and validated it with the Manning formula. Our analysis of infrared imagery and power spectral density showed a strong correlation between debris flow seismic energy and its frequency spectrum, supporting the accuracy of using seismic signals to reconstruct debris flow events. This study provides a foundation for real-time monitoring, analysis, early warning, and hazard assessment in debris flow monitoring systems based on seismic signals.

Highlights:

- Real-time monitoring of debris flow kinematics based on seismic signals.
- Extraction of debris flow characteristics (e.g., peak velocity) over space/time.
- Provides a framework for upscaling debris flow monitoring networks.

https://doi.org/10.5194/egusphere-2024-2977
Preprint. Discussion started: 29 October 2024

1 Introduction

Landslides involve the movement of rock and soil on slopes, slipping along shear surfaces (Yan et al., 2020). In contrast, debris flows are solid-fluid mixtures that can create destructive surges during heavy rainfall (Iverson, 1997). Recent incidents include a debris flow in Zhouqu County, China, on August 7, 2010, which caused 1,765 deaths and damaged over 5,500 homes (Tang et al., 2011), and another in Montecito, California, on January 9, 2018, resulting in 189 casualties and damage to 408 houses (Kean et al., 2019). Due to the high risk associated with debris flows, there is significant interest in disaster reduction measures, particularly seismic and flow depth monitoring systems. On-site monitoring is crucial for understanding the triggers of debris flows, such as rainfall, and for gathering key data like flow depth and velocity, which are essential for effective warning systems (Tecca et al., 2003; Suwa et al., 2009; Hürlimann et al., 2019).

Current monitoring and early warning systems focus on factors that trigger and evolve debris flows, primarily rainfall, with early warning thresholds based on rainfall intensity or duration (Chien-Yuan et al., 2005; Chen et al., 2007; Hürlimann et al., 2014, 2019; Cui et al., 2018; Liu et al., 2021). Hürlimann et al. (2014) suggest using a combination of average rainfall intensity and duration to define thresholds. Cui et al. (2018) proposed a method to differentiate debris flows from floods based on rainfall data. However, relying on historical rather than real-time rainfall data complicates threshold determination and reduces the transferability of these systems.

Alternative approaches use flow velocity and depth as primary indicators for monitoring and early warning (Marchi et al., 2002; Kogelnig et al., 2014; Hürlimann et al., 2019). These measurements can be combined with section geometry to estimate discharge and analyze characteristics like grain size (Arattano and Marchi, 2008; Hürlimann et al., 2019). Radar and ultrasonic instruments effectively measure flow depth and velocity (Arattano and Moia, 1999; Kogelnig et al., 2014), allowing for easy determination of early warning thresholds. However, installing ultrasonic sensors above channels can be challenging. Berti et al. (2000) noted changes in hydrological

https://doi.org/10.5194/egusphere-2024-2977
Preprint. Discussion started: 29 October 2024

characteristics over time in Acquabona Creek, while Hürlimann et al. (2003) observed varying properties among different debris flows in the Swiss Alps, showcasing the effectiveness of ultrasonic and radar devices for monitoring.

It is critical to assess sites for monitoring systems in advance to ensure proper instrumentation. A variety of instruments, including infrasound sensors (Marchetti et al., 2019), LiDAR (Aaron et al., 2023), fiber optic sensors (Huang et al., 2012; Schenato and Pasuto, 2021), pressure sensors (Berti et al., 2000; Kean et al., 2012), and stress sensors (McArdell et al., 2007; McCoy et al., 2010; Nagl and Hübl, 2017), are increasingly utilized to capture a wide array of parameters. Belli et al. (2022) found that physical parameters of debris flows correlate positively with seismic signal amplitudes. However, the sudden and intense nature of debris flow surges can damage close-range monitoring instruments, complicating data collection.

New monitoring methods are urgently needed to enhance debris flow monitoring, and recent advancements in environmental seismology provide a promising approach (Hibert et al., 2011; Moretti et al., 2012; Ekström and Stark, 2013; Barrière et al., 2015; Dammeier et al., 2016; Cook and Dietze, 2022). This field can detect ground vibrations from natural hazards as seismic signals, which have been applied to monitor various geological events, including landslides (Li et al., 2017; Fuchs et al., 2018), rockfalls (Deparis et al., 2008; Vilajosana et al., 2008), avalanches (Schneider et al., 2010; Van Herwijnen and Schweizer, 2011), as well as debris flow (Arattano, 1999; Burtin et al., 2009; Schimmel and Hübl, 2016; Walter et al., 2017; Lai et al., 2018). The main benefits of environmental seismology are long-distance monitoring capabilities and detailed event dynamics (Arattano and Marchi, 2008; Hübl et al., 2013; Kogelnig et al., 2014). Seismic monitoring can capture detailed event evolution, vital for analyzing movement characteristics and issuing warnings. Walter et al. (2017) successfully detected a debris flow half an hour before it reached a critical point, while Lai et al. (2018) proposed a method for calculating flow velocity and distance from seismic signal characteristics. Farin et al. (2019) introduced a model for estimating parameters related to debris flow

https://doi.org/10.5194/egusphere-2024-2977
Preprint. Discussion started: 29 October 2024

dynamics, and Andrade et al. (2022) found a linear relationship between seismic signal amplitude and debris flow rate. Ongoing research focuses on event timing, location, parameter evolution, and detection to improve early warning systems (Schimmel and Hübl, 2016; Lai et al. al., 2018; Beason et al., 2021; Andrade et al. 2022; Schimmel et al., 2022).

However, high-frequency seismic signals from debris flows are challenging to detect due to their rapid attenuation and short propagation distances. These signals are often only recorded by close-range instruments (Zhang, 2021). For instance, the Zhouqu debris flow's high-frequency signals were captured by nearby seismic stations (Huang et al., 2020). Near-field stations can provide detailed information on debris flow events, while far-field stations offer a broader overview (Cook and Dietze, 2022). Remote monitoring primarily relies on low-frequency seismic signals, which are less attenuated over distance and provide a better signal-to-noise ratio (Huang et al., 2008; Cook et al., 2021). Unlike landslides, debris flows lack significant low-frequency features in seismic signals, making remote monitoring impractical. Understanding debris flow seismic signals and their development processes is limited, but near-field seismic monitoring offers more detailed insights, enhancing event analysis. Therefore, near-field monitoring is the preferred method.

Debris flows usually occur in mountainous regions (Tang et al., 2011), such as Er Gully (Guo et al., 2016; Cui et al., 2018), where transportation is limited, complicating the installation of monitoring equipment. These areas often lack electricity, making battery-powered instruments necessary, which is challenging in remote locations. Solar energy could help address these electricity shortages, but inadequate sunlight in mountainous areas may hinder the operation of high-power monitoring devices. Thus, there is an urgent need to explore affordable, reliable, and convenient methods for effective debris flow monitoring.

As for characteristics of debris flow in the western part of China, we designed a near-field debris flow monitoring system, which is comprised of seismic equipment,

https://doi.org/10.5194/egusphere-2024-2977
Preprint. Discussion started: 29 October 2024

rainfall gauge, and infrared camera, and monitored three debris flows on August 19, 2022, in the Wenchuan Earthquake area of China. Then, we do a comprehensive analysis of recovered seismic data, infrared imagery, post-event field investigation, and rainfall data and gain semi-quantitative data on the debris flow. The study offers a framework for establishing debris flow monitoring and semi-quantitative analysis based on seismic signals. It introduces a cost-effective, dependable, and convenient approach for monitoring debris flows in intricate mountainous terrains.

2 Study site and field monitoring system

2.1 Study area

The study area is located in Wenchuan County, Sichuan Province, China (Figure 1), characterized by north-northeast trending mountains divided by the Minjiang River and its tributaries. This region, formed by tectonic uplift and river erosion, features undulating terrain, ravines, and steep slopes. River gradients range from 5° to 30°, while hillslope gradients range from 25° to 50°. The climate is humid, with annual rainfall between 800-1200 mm (Guo et al., 2016). The area experiences frequent seismic activity, and signs of the May 12, 2008, Wenchuan Earthquake are still evident, with loose rocks and soils providing abundant sediment for debris flows. This study focuses on the Er and Fotangba Gullies in the Minjiang River Basin, which has experienced numerous debris flow events in recent years, threatening nearby villages, roads, and hydropower stations. Notable incidents include 17 documented events by Guo et al. (2016), as well as specific events like the debris flow in Er Gully on July 10, 2013 (Guo et al., 2016), in Fotangba on the same date (Cao et al., 2019), and another in Er Gully on July 5, 2016 (Cui et al., 2018).

https://doi.org/10.5194/egusphere-2024-2977
Preprint. Discussion started: 29 October 2024

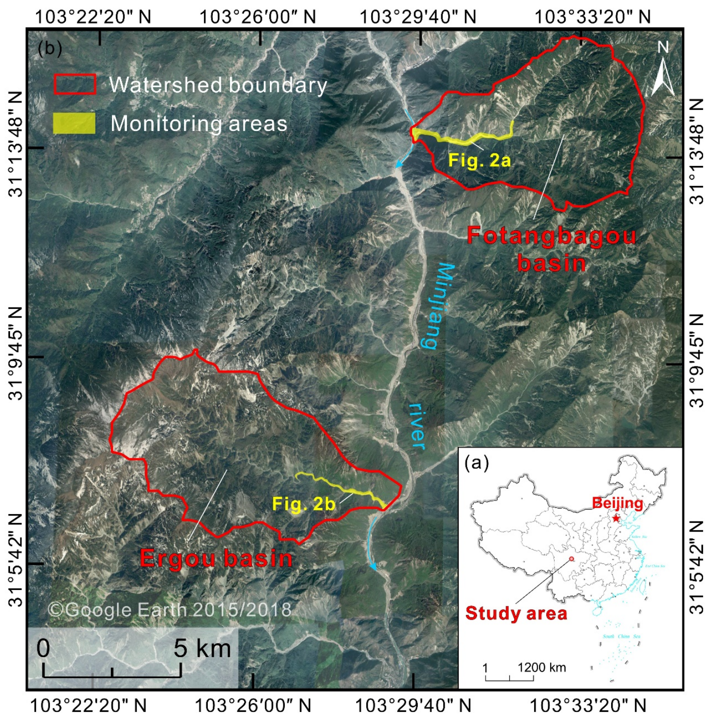

Figure 1 Overview of the study area. (a) Location of the study area within China; (b) The two study catchments, Er and Fotangba Gullies, on the Minjiang River, Wenchuan, Sichuan, China.

Er Gully drains an area of 39.4 km^2 and is about 6 km from the epicenter of the Wenchuan Earthquake; it ranges in altitude from 930 to 4120 m, has a channel length of about 12 km, an average slope of about 12°, and a debris flow transportation area of between 5 to 12° (Guo et al., 2016). The Gully is located on the right bank of the Minjiang River and drains west to east, with steep walls, a narrow and winding channel, and abundant water sources. The average slope is 10.5°. Important nearby infrastructure at risk includes a factory at the end of the Gully, a village on the left bank of the Minjiang River facing the Gully mouth, and national highway G213 adjacent to the bank.

The Fotangba Gully basin has an area of 33.6 km^2; it ranges in altitude from 1117–

https://doi.org/10.5194/egusphere-2024-2977
Preprint. Discussion started: 29 October 2024

3462 m, has a channel length of about 9.78 km, and has bank slopes of 25–45° (Cao et al., 2019). The Gully is on the left bank of the Minjiang River and drains east to west. The Gully has abundant water sources, with steep walls and a wide and gently winding channel. The average slope is 6.1°. There are hydropower stations on the Minjiang River near the Gully and on the north side of the Gully mouth.

2.2 Monitoring systems

We have developed a near-field debris flow monitoring system with seismic monitoring devices, infrared cameras, and precipitation gauges. This system provides a cost-effective, reliable, and practical solution for debris flow monitoring. It primarily utilizes seismic signals and infrared camera images to comprehensively monitor the debris flow process, while precipitation gauges provide real-time precipitation data. Infrared cameras with 5-min interval shooting have a lower electric power consumption than infrared videos with better-infrared monitoring range and higher resolution, which is available in our study area. Infrared cameras are cheap, plus solar energy about $ 78, and Hikvision 's infrared video camera plus solar energy about $ 425. Hikvision's infrared video camera (Type: DS-2CD3T46WDV3-L) exhibits high power consumption. The power generated by the solar panel is only sufficient to sustain continuous video monitoring for approximately 74 hours. Infrared cameras, which are equipped with solar cells and eight 1.5-volt dry batteries, can provide continuous monitoring for up to 18 months.

This near-field debris flow monitoring system is well suited for complex mountainous regions with little sunlight and difficult power supply conditions. The placement of the instruments requires the selection of unobstructed locations along the banks of the canyon to ensure a wide field of view, while the seismic monitoring equipment should be installed on stable bedrock or on poured concrete piers to ensure sufficient solar power supply, wide video recording angles, and accurate seismic data. Wenchuan has an average annual sunshine duration of around 1693.9 to 1042.2 hours (Huang et al., 2018). The monitoring instruments in Fotangba Gully are installed on the

https://doi.org/10.5194/egusphere-2024-2977
Preprint. Discussion started: 29 October 2024

left bank of the channel, which is about 90 meters wide and has a left-sided slope of about 40 degrees. According to rough estimates on site, the daily solar radiation in summer is about 6 hours. The earthquake monitoring system was in continuous operation at most from July 2023 to March 2024, which corresponds to a monitoring period of 9 months. In other, relatively narrow gullies, the daily solar radiation in summer is around 4 to 5 hours, and the seismic monitoring system is monitored continuously for at least 4 months in each case.

The monitoring system has been implemented in multiple Gullies in Wenchuan County, China, including Fotangba Gully, Er Gully, and Mozi Gully, and successfully recorded debris flow events. Two monitoring stations were established in both Fotangba and Er gullies. In Fotangba, Station 1 is 3,260 meters from the valley entrance, while Station 1 in Er Gully is 4,130 meters from the entrance (Table 1, Figure 2). The distance between the two monitoring stations in Fodangba Gorge is about 520 meters, with both stations installed on platforms on the left bank of the channel, about 20 meters from the middle of the channel, where they are located on exposed rock. In the Er Gully Gorge, which is about 460 meters long, the measuring stations are installed on platforms on the right bank slope, about 15 meters from the middle of the channel. All data is recorded in real-time; however, due to the lack of a network signal, data transmission via the Internet/GSM is not possible. The seismic monitoring equipment operates at a sampling frequency of 100 Hz, while the infrared cameras are set to record at 5-minute intervals, with specific parameters listed in Table 1. This monitoring system captures seismic signals, images, and real-time precipitation data throughout the debris flow process and provides reliable data to support the reconstruction and dynamic analysis of debris flows.

https://doi.org/10.5194/egusphere-2024-2977
Preprint. Discussion started: 29 October 2024

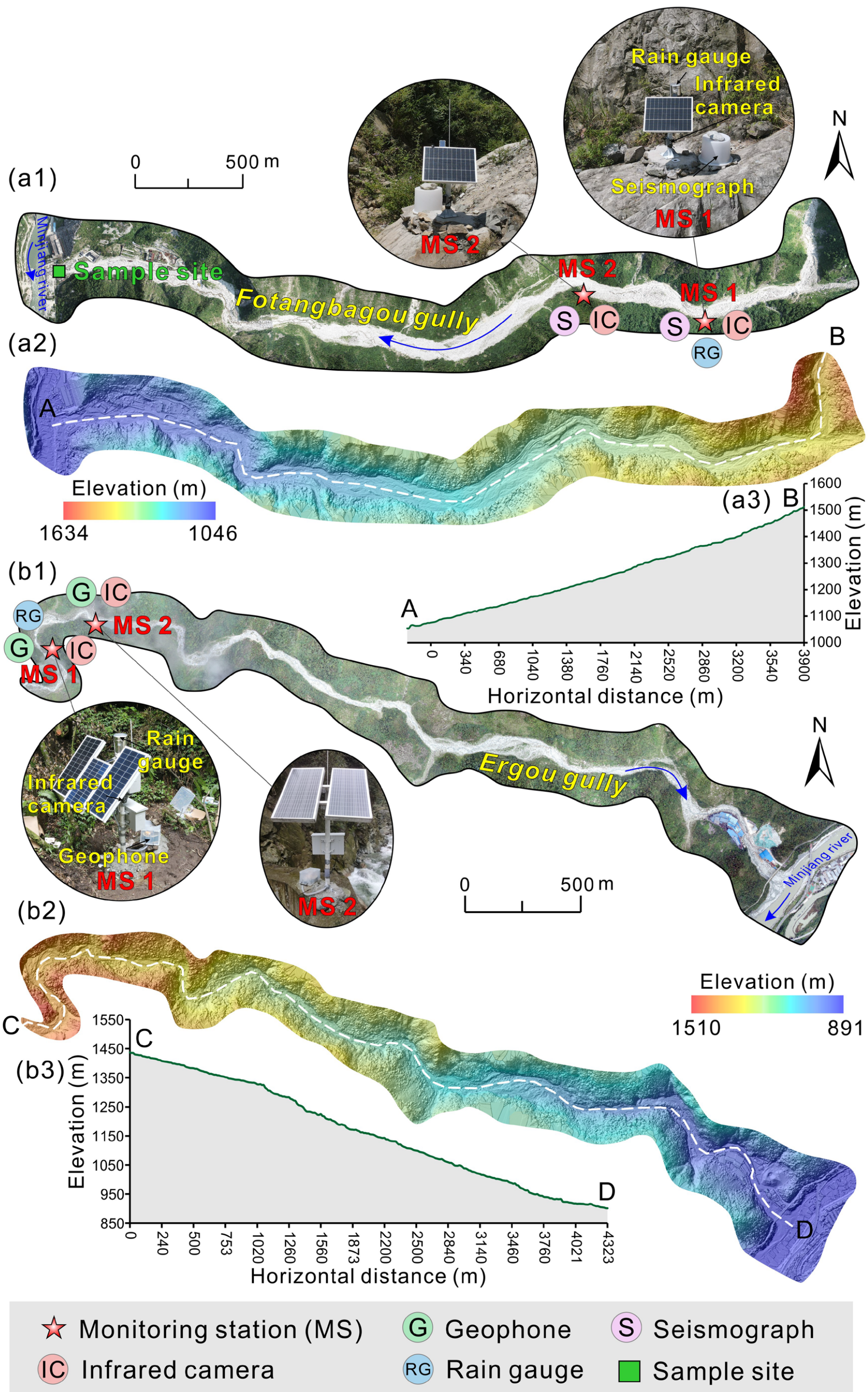

224

225 **Figure 2** Schematic overview of monitoring network layout in the two study

https://doi.org/10.5194/egusphere-2024-2977
Preprint. Discussion started: 29 October 2024

catchments. (a) Fotangba Gully: (a1) drone aerial photography, (a2) Digital Terrain Model map, (a3) longitudinal profile; (b) Er Gully: (b1) drone aerial photography, (b2) Digital Terrain Model map, (b3) longitudinal profile. See Figure 1 for Gully locations.

Table 1 Instrument parameters for monitoring stations in the two study catchments.

Equipment	Instrument parameters	
	Fotangba Gully	Er Gully
Seismograph (NOISESCOPE)	Sampling rate 100 Hz Corner frequency not offered Power consumption: <3 W	—
Geophone (DATA-CUBE^3)	—	Sampling rate 100 Hz Corner frequency of 4.5–150 Hz Power consumption: 128mW
Rain gauge	Record once per hour with a resolution of 0.2 mm	
Infrared camera	1 shot every 5 minutes at 2592×1944, 1920×1080 dpi resolution during the day and at night Continuous shooting: ≥18 months	

3 Methodology

Process and interpret debris flow seismic signals according to the steps in Figure 3 to extract information on the evolution of debris flow. Firstly, perform absorption attenuation compensation on the extracted debris flow seismic signals to restore energy loss caused by propagation differences and obtain debris flow seismic signals unaffected by sensor placement. Next, generate seismic spectrograms using the short-time Fourier transform to conduct characteristic analysis of debris flow evolution, and estimate the maximum velocity of debris flow through cross-correlation functions. Analyze the results using infrared imagery and on-site investigations. Finally, analyze the particle and flow velocity characteristics of debris flow by calculating the power spectral density of keyframes. The amplitude method is used to obtain the absolute

https://doi.org/10.5194/egusphere-2024-2977
Preprint. Discussion started: 29 October 2024

value of time-domain amplitude, and the processed signal is referred to as a simplified signal (Arattano and Moia, 1999).

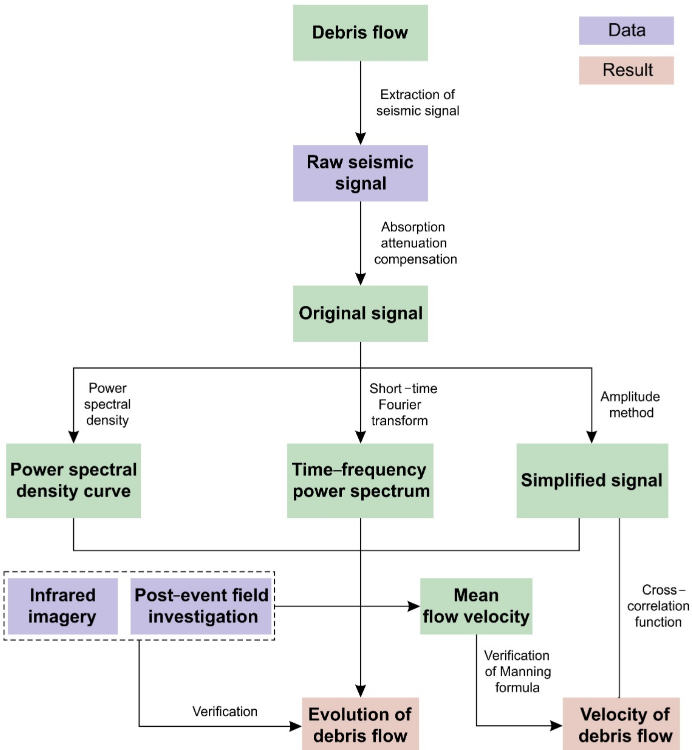

Figure 3 Research methodology for processing and analysis of debris flow seismic signal.

3.1 Short-time Fourier transform

The short-time Fourier transform (STFT, Eq. (1)) is used to analyze the time-frequency domain characteristics of the debris flow seismic signal (Yan et al., 2021, 2022, 2023). The method allows the time domain and frequency domain characteristics of the signal to be analyzed simultaneously:

$$X(t, \omega) = \sum_{m=-\infty}^{\infty} x(m) W(t-m) e^{-j\omega m}, \qquad (1)$$

where X and x are signals of time-frequency and time domain, W is the window function,

https://doi.org/10.5194/egusphere-2024-2977
Preprint. Discussion started: 29 October 2024

m is the start time of the window function, *ω* is the angular frequency, *e* is a natural constant, *t* is time, and *j* is the imaginary number (Yan et al., 2021). A Hanning window length of 2056 and a time length of 20.56 s correspondingly is used. A built-in function "spectrogram" of MATLAB is used to achieve STFT directly from the software manual.

3.2 Cross-correlation function

The cross-correlation function is used to compute the time delay of τ that corresponds to the travel duration of the source between the stations. The time delay of the signals comes from sampling signals, such as M signal samples $[x_K]$, $[y_K]$ in Eq. (2) and (3) at different locations when the maximum calculation result $\phi_{yx}(\tau)$ is obtained based on Eq. (4) (Arattano and Marchi, 2005). Arattano and Marchi (2005) proposed that the value of the velocity computation is close to the value of the velocity measurement. In the context of debris flows, the average flow velocity between monitoring stations can be obtained by dividing the distance between the stations by the signal time delay. This method has been used to objectively calculate the mean velocity of debris flows (Coviello et al., 2015):

$$\left[x_K\right]=\left[x_0,x_1,x_2,\ldots,x_{M-1}\right] \tag{2}$$

$$\left[y_K\right]=\left[y_0,y_1,y_2,\ldots,y_{M-1}\right] \tag{3}$$

$$\phi_{yx}(\tau)=\sum_{t=0}^{M-1} x_t y_{t+\tau} \ , \tag{4}$$

where y from station 2 is another signal of time domain for the same event as x from station 1, t and K which are absolute sampling time series from 0 to M-1, ϕ represent cross-correlation function. When t exceeds M-τ-1 and is less than 0, x_t and $y_{t+\tau}$ is equal to 0.

3.3 Power spectral density

Power spectral density (PSD, Eq. (5)) can be used to estimate power per frequency for different frequencies in a specific period (Yan et al., 2020), and allows debris flow evolution to be analyzed from the seismic signal.

https://doi.org/10.5194/egusphere-2024-2977
Preprint. Discussion started: 29 October 2024

$$PSD_{f_{\min}\sim f_{\max}}(t)=\frac{1}{(f_{\max}-f_{\min})}\times\sum_{f=f_{\min}}^{f_{\max}}X(t,f), \qquad (5)$$

where $f_{\min}$ and $f_{\max}$ represent minimum frequency and maximum frequency, respectively, t is time for the seismic signal, and $X(t, f)$ represents the spectrogram based on STFT (Yan et al., 2017). The sampling rate is 100 Hz, so we choose 1 Hz and 50 Hz (i.e., a half of 100 Hz) as $f_{\min}$ and $f_{\max}$.

PSD can be calculated by Eq. (6) based on seismic signals (Lai et al., 2018). PSD has a link with transporting bed load in rivers, Roth et al. (2016) provide insight into that the component signals come from water turbulence, rainfall, and sediment transport. It gives us a research direction about applying PSD to studying debris flows.

$$PSD\approx 1.9\cdot LWD^3u^3\cdot\frac{f^{3+5\xi}}{v_c^5 r_0}e^{-\frac{8.8f^{1+\xi}r_0}{v_cQ}}, \qquad (6)$$

where W is width of the channel, D represents the 94th centile of the grain size distribution, u represents debris flow velocity, f is frequency, v_c is Rayleigh wave phase velocity at 1 Hz, r_0 is distance between the monitoring station and channel, L is effective length of L=r_0, ξ=0.4 is a parameter related to how strongly seismic velocities increase with depth at the site, and Q is an attenuation factor (Tsai et al., 2012; Lai et al., 2018).

3.4 Absorption attenuation compensation

Elastic wave travel makes energy and velocity smaller. The two effects are a function of frequency and are mathematically expressed by Eq. (7) with some parameters (Kjartansson,1979; Futterman, 1962; Strick,1967). It can be used to restore a part of energy loss as:

$$h(t,f)=e^{-\frac{\pi ft}{Q}\left|\frac{\omega_0}{\omega}\right|^{\frac{2}{\pi}\arctan\left(\frac{1}{2Q}\right)}}, \qquad (7)$$

where f is the frequency of the seismic signal, t is the spreading time (i.e., 0.02 s and 0.05 s) which is equal to distance r_0 between the monitoring station and channel divided by Rayleigh wave velocity v_c in Eq. (6), Q represents attenuation factor quantitatively depicting the absorption attenuation, and ω_0 and ω are reference angular velocity at 1

https://doi.org/10.5194/egusphere-2024-2977
Preprint. Discussion started: 29 October 2024

Hz (ω_0=2π) and angular velocities, respectively.

$$\Gamma(t,f)=\frac{h(t,f)+\sigma^2}{h^2(t,f)+\sigma^2}, \tag{8}$$

where σ is a constant named stability control factor, whose value comes from a numerical experiment., with a σ^2 value of 0.02 used here.

The high-frequency signal can be restored by Eq. (8) better with a comparison of Eq. (7). Because the seismic signal of debris flow belongs to a high-frequency signal, we always use Eq. (8) at all the frequencies of 1 Hz to 50 Hz.

4 Results and analysis

4.1 Debris flow seismic energy recovery and process reconstruction

4.1.1 Debris flow seismic and rainfall data

This study effectively captured seismic signals from three debris flows that occurred on August 19, 2022, in the Fotangba and Er gullies using a near-field monitoring system. After preprocessing the raw data, we analyzed the vertical component (Figure 4). The seismic signals recorded by the monitoring system exhibited significant amplitude increases and fluctuations during the debris flow events. The analysis revealed two debris flows in the Fotangba Gully and one in the Er Gully. The spectrograms and amplitude trends at both monitoring stations displayed similar characteristics of rapid increase followed by gradual decrease. Notably, the second debris flow in Fotangba exhibited greater amplitude and duration compared to the first, with more pronounced signal variations observed at monitoring station 1 than at station 2. In Er Gully, monitoring station 2 recorded higher amplitudes and fluctuations in seismic signals compared to station 1, which can be attributed to the instrument layout and site conditions. We calculated the signal-to-noise ratios (SNR) for the debris flows at different monitoring stations. The SNRs for the first debris flow in Fotangba were 20.66 dB and 7.96 dB at the two stations, while the second debris flow had SNRs of 19.60 dB and 15.80 dB. In Er Gully, the SNRs were 20.47 dB and 17.62 dB at the two

https://doi.org/10.5194/egusphere-2024-2977
Preprint. Discussion started: 29 October 2024

stations. All three debris flows showed relatively high SNRs. The analysis indicated better seismic signal quality at Fotangba monitoring station 1 and Er Gully monitoring station 2. Given the larger magnitude, longer duration, and smaller channel bends of the second debris flow in Fotangba. The following research will focus on a more detailed analysis and reconstruction of this event.

The rainfall record for Fotangba Gully shows hourly rainfall of 6.4 mm and 14.2 mm before the first and second debris flows, respectively (Figure 4e). In Er Gully, the hourly rainfall before the debris flow was 3.8 mm (Figure 4f). Analysis indicates precipitation occurred before the three debris flows. Additionally, the rainfall data can be linked to the initiation time of the flows and significant changes in seismic signals. The two debris flows in Fotangba Gully coincided with the maximum hourly rainfall on the day of the events (second highest and highest) within 24 hours, while the Er Gully debris flow did not coincide with a maximum. However, the cumulative rainfall before the Er Gully debris flow reached 15 mm, greater than the cumulative rainfall for the first debris flow in Fotangba Gully. Therefore, rainfall is considered the triggering factor for debris flow initiation in both gullies.

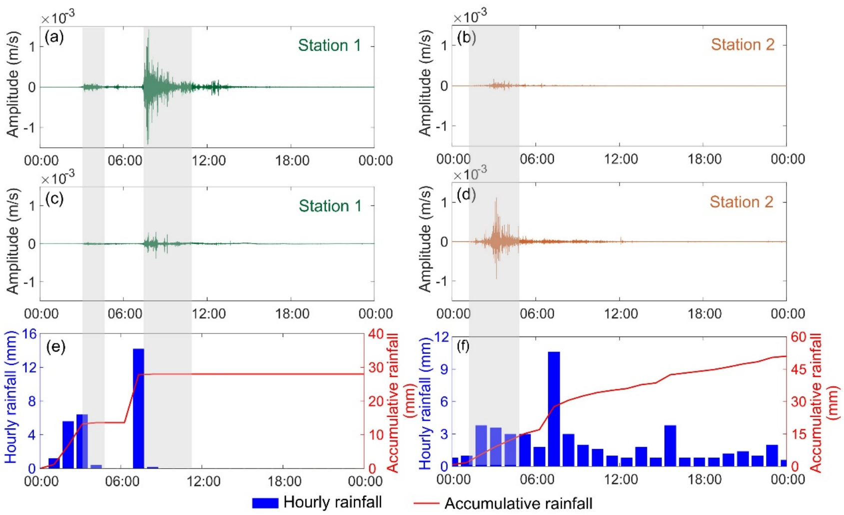

Figure 4 The seismic signals and rainfall of the debris flow in their raw form. (a) and (c) represent monitoring station 1 and station 2 in the Fotangba Gully; (b) and (d)

https://doi.org/10.5194/egusphere-2024-2977
Preprint. Discussion started: 29 October 2024

represent monitoring station 1 and station 2 in the Er Gully; (e) Rainfall at Fotangba Gully; (f) Rainfall at Er Gully.

4.1.2 Debris flow seismic energy recovery

We applied Eq. (7) and (8) to compensate for the maximum possible energy loss during the propagation of debris flow seismic signals. These signals were recorded along the river channel. As the debris flow travels through the channel, it generates vibration signals that propagate to the monitoring stations and are recorded by sensors. This seismic signal is a superposition of the vibration signals generated by the entire debris flow, characterized as a "line source." To accurately reproduce the energy of this "line source" seismic signal, it is essential to precisely determine the propagation paths of individual "sources." However, due to factors such as river channel morphology and surface velocity variations, this information is challenging to ascertain accurately. To simplify the compensation process, we considered the area within 50 meters upstream and downstream of the monitoring station as the primary sources of the seismic signals recorded at the station. We calculated the geometric mean of seismic wave propagation times from the center of this 50-meter river channel to the monitoring station at 0.5-meter intervals, using this geometric mean as the seismic wave propagation time for energy compensation. Another important parameter is the velocity and amplification factor (σ^2) of the 1 Hz Rayleigh surface wave, which is influenced by the geological conditions near the monitoring station. Since we performed near-field observations, we neglected velocity variations near the station and assumed that the velocity of the 1 Hz Rayleigh surface wave remains constant. This assumption simplifies the geometric mean of the transit times to the geometric mean distance of this flux section relative to the observation point. The amplification factor (σ^2), ensuring numerical stability, was determined through numerical experiments. The principle of these experiments was to expand the compensation frequency range as much as possible while maintaining a high signal-to-noise ratio for the debris flow signal.

https://doi.org/10.5194/egusphere-2024-2977
Preprint. Discussion started: 29 October 2024

Based on the second debris flow event in Fotangba Gully, we analyzed the surface conditions near the site and conducted practical investigations of near-surface velocities in the bank areas using petroleum seismic techniques (Liu et al., 2013). This analysis allowed us to determine the Q values and reference velocities for two specific locations in Fotangba Gully. The Q values were found to be 4 and 2.4, with corresponding Rayleigh wave velocities of 800 m/s and 500 m/s at a frequency of 1 Hz. We calculated the geometric mean travel times for these two locations to be 0.02 seconds and 0.04 seconds, respectively. After numerous numerical experiments, we set the gain control factors for both locations to 0.02. There is only limited reference material available for the standard velocity of surface waves. To estimate this velocity, we refer to the results of surface surveys during seismic exploration of petroleum deposits. These estimates may vary, but the principle we apply in our practical compensation "maximizing energy in all frequency bands while maintaining numerical stability" allows us to correct any discrepancies during the actual compensation process (Yang et al., 2019).

From the compensation spectrum curve, the high-frequency components have been significantly restored, and both sites show similar improvements in their spectrum curves (Figure 5). The time domain curve indicates that the characteristic changes at site 2 after compensation further enhances its similarity to site 1, with these changes being more pronounced. In terms of effectiveness, the compensation has proven to be quite effective, as it mitigates the absorption attenuation of the debris flow seismic signals to some extent. Therefore, in the following sections, we will use the compensated seismic signals for further analysis of the second debris flow event at Fotangba Gully.

https://doi.org/10.5194/egusphere-2024-2977
Preprint. Discussion started: 29 October 2024

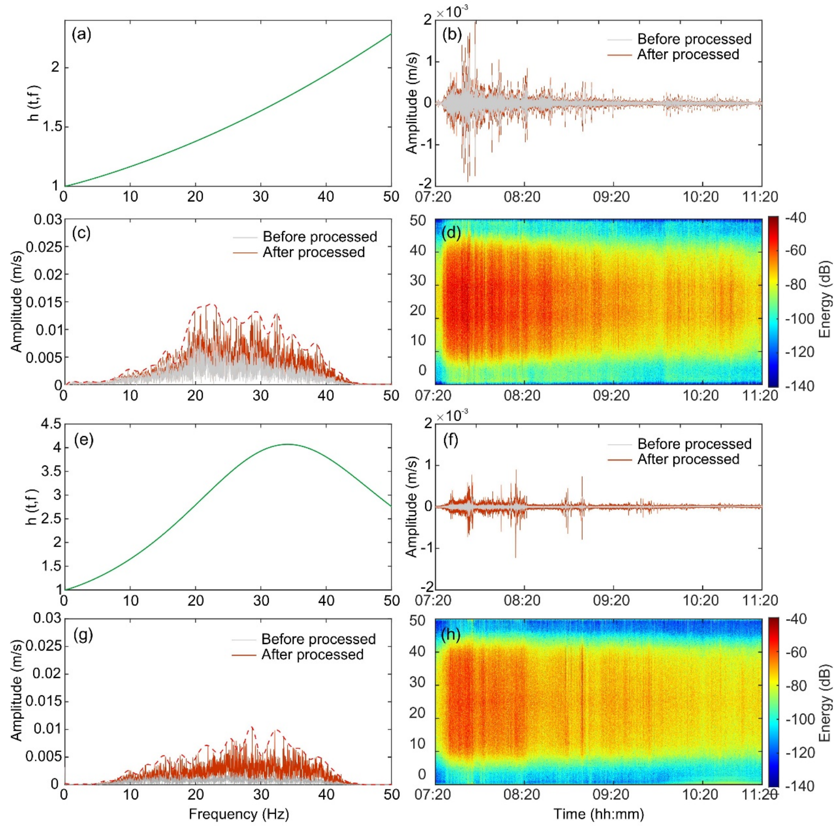

Figure 5 Restored seismic signal for the second debris flow in Fotangba Gully. (a) Compensation function curve for monitoring station 1; (b) Time domain signal at monitoring station 1; (c) Frequency domain signal at monitoring station 1; (d) Restored spectrogram for monitoring station 1; (e) Compensation function curve for monitoring station 2; (f) Time domain signal at monitoring station 2; (g) Frequency domain signal at monitoring station 2; (h) Restored spectrogram for monitoring station 2. The red dashed lines in (c) and (g) are envelopes that represent peak amplitudes after processing.

4.1.3 Process reconstruction by seismic

Through the analysis of section 4.1.1, we selected data from Fotangba station 1 and Er Gully station 2, which had high-quality signal records, for further time domain and time-frequency spectral analysis (Figure 6). Notably, at Fotangba Gully, the second

https://doi.org/10.5194/egusphere-2024-2977
Preprint. Discussion started: 29 October 2024

debris flow event shows more significant amplitude changes and energy release compared to the first. The time-frequency spectral analysis further indicates that the scale and duration of the second debris flow event exceeded those of the first.

By monitoring the abrupt changes in amplitude and frequency spectra of seismic signals, we can estimate the start and end times of debris flow events. As shown in Figure 6, the seismic signals in Fotangba Gully experienced a sharp increase in amplitude and energy around 3:07 a.m., stabilizing around 5:26 a.m., lasting approximately 2.5 hours. Then, around 7:25 a.m., the signals changed again, returning to stability around 11:24 a.m., lasting about 4 hours. In Er Gully, the seismic signals began to change around 2:44 a.m. and stabilized around 4:49 a.m., lasting approximately 2 hours. By combining information from local villagers about debris flows, we determined the specific start and end times of the three events (Table 2). Additionally, images from time-lapse cameras provided strong support for determining the start and end times of these events.

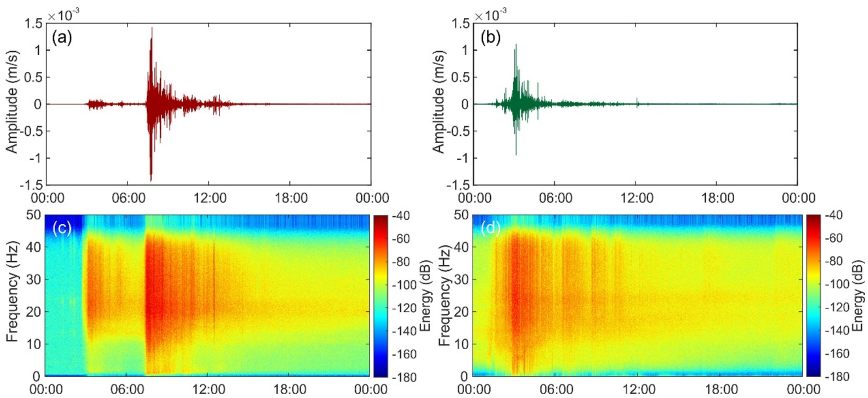

Figure 6 Time domain and time-frequency spectrum of debris flow ground motion signal. (a) and (c) Fotangba monitoring station 1; (b) and (d) Er Gully monitoring station 2.

Table 2 Starting and ending time of three debris flow events at Wenchuan, China (August 19, 2022), picked from the seismic signals.

	Fotangba Gully		Er Gully
	1st	2nd	
Starting	03:07 am	7:25 am	2:44 am
Ending	05:26 am	11:24 am	4:49 am

To investigate the seismic manifestation of the second debris flow evolution in Fotangba Gully, we processed seismic signals according to the workflow depicted in Figure 2, resulting in compensated time-domain and time-frequency spectra (Figure 7). By analyzing characteristics such as amplitude profiles, average amplitudes, and vertical spectra, we attempted to reconstruct the debris flow's evolution.

At Monitoring Point 1, the debris flow onset was recorded at 7:25, with subsequent rapid increases in signal amplitude and frequency range. Amplitudes peaked around 7:42 and then gradually declined; the frequency range associated with high power increased rapidly from 8 to 43 Hz post-debris flow initiation, maintaining high power at 22 Hz until 8:45. Monitoring Point 2 data broadly aligned with Point 1, noting a debris flow onset at 7:26, with peak amplitudes occurring around 7:45, followed by a gradual decline. However, slight differences in frequency bandwidth were observed, concentrated between 10-40 Hz from 7:30 to 7:50. Combining seismic signal characteristics from both points, the debris flow commenced around 7:25, progressively escalating in scale, reaching peak magnitudes at approximately 7:42 and 7:45 at Points 1 and 2, respectively, and subsequently stabilizing, with the entire event lasting about 4 hours. Throughout the debris flow event, peak frequencies observed at both monitoring points were 21.6 Hz and 28.6 Hz, with frequency evolution between points indicating an increase in peak frequency, potentially due to varying particle impacts and scale. Factors such as rockfall and channel erosion may also influence peak frequencies. The surge reflects the wave nature of the debris flow, and the number of surges is consistent

https://doi.org/10.5194/egusphere-2024-2977
Preprint. Discussion started: 29 October 2024

with the number of waves. The flow depth between the surges is significantly discontinuous, with a sudden increase in flow depth from one surge to the next, similar to the flow characteristics of the surge. Monitoring Points 1 and 2 observed 8 and 7 significant surges, respectively, with different numbers. Additionally, we found that Monitoring Point 2 recorded two significant surges around 9:00, while Monitoring Point 1 did not observe notable surges at that time. This indicates changes in debris flow movement characteristics along the channels of Monitoring Points 1 and 2, potentially due to variations in channel topography and solid-phase material content of the debris flow.

Overall, the trends in the time-domain and time-frequency spectra at the two monitoring points are similar, exhibiting rapid increases followed by gradual declines, consistent with the overall movement of the debris flow. However, Monitoring Point 1 recorded higher average amplitudes, wider frequency bands, and stronger energy. This may be attributed to the shorter distance between Monitoring Point 1 and the Gully, resulting in less energy loss during the propagation of seismic signals from the debris flow. Additionally, varying geological conditions may also contribute to the differences in seismic signal attenuation between the two monitoring points.

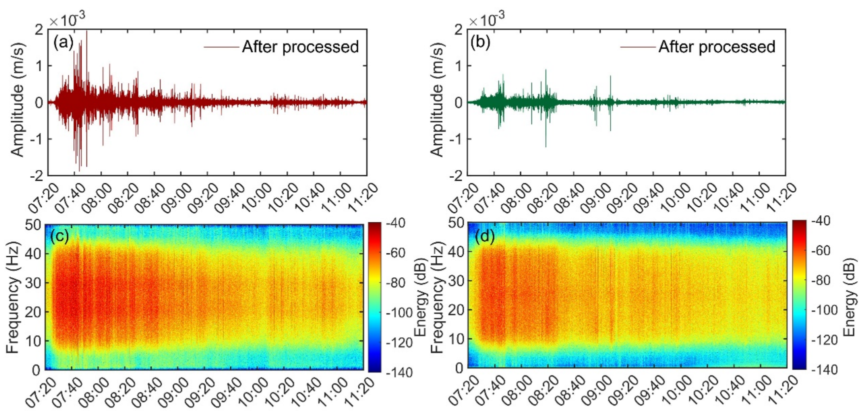

Figure 7 Restored seismic signal for the second debris flow in Fotangba Gully. (a) Time domain signal at monitoring station 1; (b) Time domain signal at monitoring station 2; (c) Time-frequency domain energy spectrum for monitoring station 1; (d) Time-

https://doi.org/10.5194/egusphere-2024-2977
Preprint. Discussion started: 29 October 2024

frequency domain energy spectrum for monitoring station 2.

4.2 Debris flow velocity analysis

Cross-correlation functions can calculate the time delay between two measuring stations for debris flows, as shown in Eq. (4). The average flow velocity can be derived from the distance between neighboring monitoring stations and this time lag. Cross-correlation functions can calculate the time delay between two measuring stations for debris flows, as shown in Eq. (4). The average flow velocity can be derived from the distance between neighboring monitoring stations and this time lag. Arattano et al. (2012), Comiti et al. (2014), and Schimmel et al. (2022) installed seismic instruments in different regions and found that the cross-correlation function can effectively calculate the debris flow velocity. In their studies, the measurement points were arranged along almost straight river channels, with the distance between the measurement points and the center of the channel being less than the straight-line distance between the measurement points. At the Fotangba Gully, the channel between points 1 and 2 is relatively flat and linear with a gradient of about 9°. The straight-line distance between these two points is 520 meters, which is greater than the 25 meters distance between the measuring points and the center of the channel. This arrangement of the instruments is similar to that in the studies mentioned above. In contrast, the river channel between the two measuring points in the Er Gully is convex (Figure 2b1) and has a gradient of around 16°. The distance between the two measuring points is approximately 460 meters, which is greater than the 200 meters straight-line distance between the two points. This instrument arrangement differs significantly from those used in previous studies. Therefore, our research mainly focuses on using the cross-correlation function to calculate the debris flow velocity at the Fotangba Gully.

Using simplified time domain signals processed with the seismic amplitude method, the φ_{yx} of the time domain signal for the second debris flow event in the Fotangba channel was calculated (Figure 8a), with a time delay τ of 74 s corresponding

https://doi.org/10.5194/egusphere-2024-2977
Preprint. Discussion started: 29 October 2024

to the maximum value of φ_{yx} for this event. The amplitude range for calculating flow velocity based on the cross-correlation function for the second debris flow event is shown in Figure 9b. The distance between monitoring sections in the Fotangba channel is 520 m, resulting in an average velocity of 7.0 m/s for the second debris flow. To further validate the cross-correlation algorithm's applicability, we calculated average flow velocities of 3.0 m/s for the first debris flow event and 38.3 m/s for the Er Gully event using the same method (Table 3). The velocity for Er Gully was significantly higher than those for the two debris flow events in Fotangba and exceeded the flow velocities of 1-6 m/s observed by Cui et al. (2018) in the S1 section, indicating it may be inaccurate.

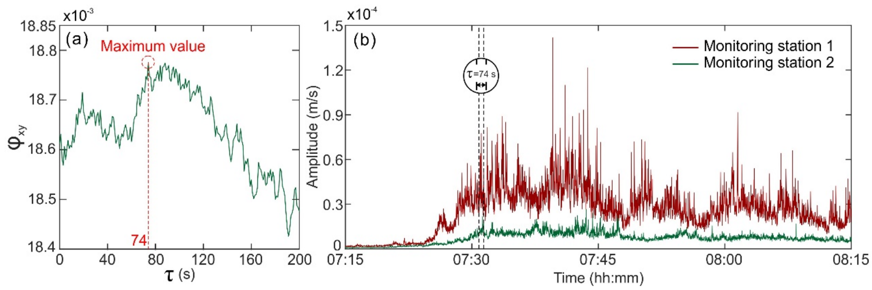

Figure 8 The cross-correlation algorithm calculates the second debris flow in Fotangba Gully. (a) signal lag time τ between two monitoring stations; (b) Amplitude range of debris flow (vertical direction).

To verify the reliability of the velocity calculations derived from the cross-correlation function, the average velocity was also computed using the Manning formula (Yu and Lim, 2003; Cui et al., 2013; Guo et al., 2016). Channel parameters were obtained from the cross-sections at the monitoring stations (Figure 9). The channel roughness coefficient *n* was set at 0.05 (Xu and Feng, 1979). The gradient ratio *J* for the monitoring section was determined from the output of the UAV aerial survey's digital surface model (DSM). For monitoring station 1, the area and wet perimeters were 17.7 m² and 14.2 m, respectively. For the other cross-section, these

https://doi.org/10.5194/egusphere-2024-2977
Preprint. Discussion started: 29 October 2024

values were 27.5 m² and 21.6 m. Consequently, the hydraulic radii *RR* for the two monitoring stations were 1.25 m and 1.27 m, respectively.

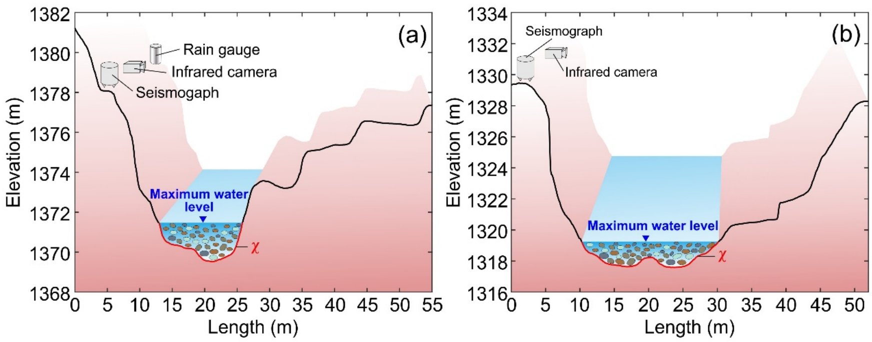

Figure 9 Cross-sections of Fotangba Gully showing maximum water level used in calculation of mean velocity by the Manning formula. (a) Monitoring station 1; (b) Monitoring station 2.

Table 3 Results of maximum velocity calculations for Fotangba Gully and Er Gully debris flows.

Debris flow	Maximum velocity calculated using each method (m/s)	
	Cross-correlation algorithm	Manning formula
First debris flow in Fotangba Gully	3.006	—
Second debris flow in Fotangba Gully	7.027	7.921
Debris flow in Er Gully	38.333	—

4.3 Analysis of debris flow reconstruction effectiveness based on seismic signals

Taking the second Fotangba Gully debris flow as an example, we will use infrared imagery and field survey data to analyze the effectiveness of the debris flow evolution process and analyze the impact of flow velocity and particle size on seismic motion signals through PSD.

https://doi.org/10.5194/egusphere-2024-2977
Preprint. Discussion started: 29 October 2024

4.3.1 Infrared imagery analysis

To verify the accuracy of reconstructing debris flow processes through seismic signals, we analyzed infrared images of the debris flows. Nighttime infrared imaging often faces limitations due to low visibility and resolution, resulting in poor image quality for the first and second Fotangba Gully debris flows during the night, making them unsuitable for analysis. To overcome these issues, we focused on the second daytime debris flow, which benefited from significantly improved image quality.

During the debris flow event, we captured infrared images at 5-minute intervals from 7:39 to 8:04 (Figure 10 b to g). Due to blurriness from water droplets on the camera lens at Monitoring Point 2, we relied solely on the infrared camera at Monitoring Point 1. The images showed that at 7:39, the debris flow volume was low, and the channel had not yet been submerged. Most of the flow is concentrated in the right channel, with less flow in the left channel. By 7:44, the debris flow began to submerge Point A and erode the left bank at Point B. Water depth and left bank erosion peaked at 7:59, after which water depth started to decrease. Overall, the infrared images indicated a gradual increase in flow from 7:39 to 7:54, followed by a decrease.

Flow velocity peaked at 7:39 and then gradually decreased, remaining relatively stable in subsequent images. The maximum turbulence at Point C indicated the highest flow velocity, which then gradually declined. The vortices near Point A suggested higher flow velocities, while the fluid patterns upstream at Point C indicated slower speeds. The vortices near Point C may have been caused by excessive discharge from lower elevations. Notable surges were observed in Figure10 b to e, particularly at 7:49 and 7:54, with significant debris flow surges. From 7:39 to 7:59, the debris flow volume gradually increased due to higher flow velocities, which eroded the sediments along the channel, enhancing solid-phase material content and flow volume. After 7:59, the reduced flow velocity led to weaker erosion and a gradual decrease in particle content, evolving into a "flood" state. The debris flow surges matched the small peaks observed in the seismic signals. The trends in particle content mirrored those of flow volume,

https://doi.org/10.5194/egusphere-2024-2977
Preprint. Discussion started: 29 October 2024

gradually increasing from 7:39 to 7:49, remaining high from 7:49 to 7:54, and significantly decreasing at 7:59 and 8:04.

Through the analysis of debris flow evolution, we found that flow volume gradually increased from 7:39 to 7:59, with flow velocity peaking at 7:39 before gradually decreasing and experiencing multiple surges. The image analysis largely matched the debris flow evolution reconstructed through seismic signals, and the corresponding image timestamps further confirmed the consistency between the characteristics of the Fotangba seismic signals and the observations from the images, supporting the accuracy of reconstructing the second Fotangba debris flow event through seismic signals. However, the peak times were not entirely consistent with the seismic data, possibly due to the 5-minute recording interval. In the next section, we will integrate these variables with forward modeling of the seismic power spectral density (PSD) generated by the debris flow to analyze their impacts on the signals, providing deeper insights into the discrepancies in peak times observed between infrared images and seismic interpretations.

https://doi.org/10.5194/egusphere-2024-2977
Preprint. Discussion started: 29 October 2024

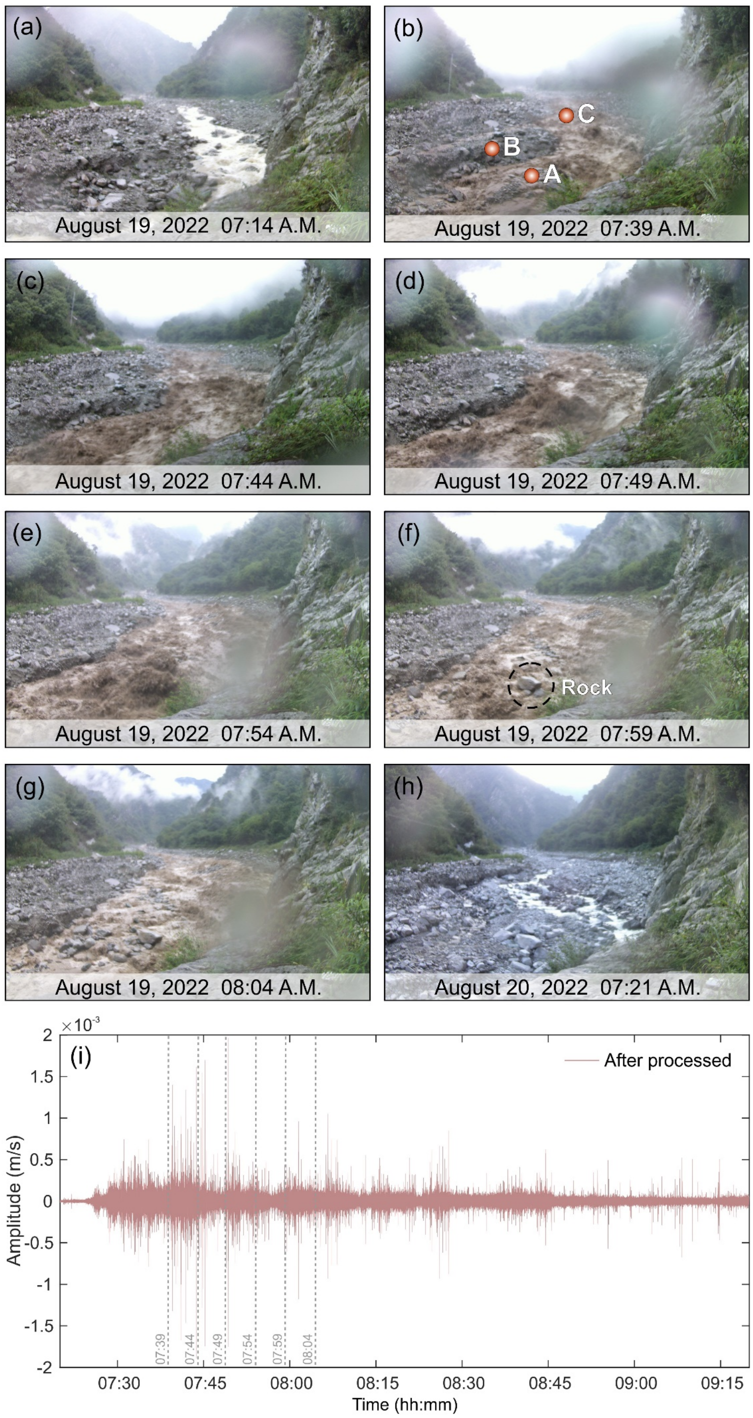

584

585 **Figure 10** Infrared camera images taken and the seismic signal recorded at monitoring

https://doi.org/10.5194/egusphere-2024-2977
Preprint. Discussion started: 29 October 2024

station 1 in Fotangba Gully during the second debris flow on the morning of August 19, 2022. Images were recorded every 5 minutes from 7:39 to 8:04: (a) 7:39 frame; (b) 7:44 frame; (c) 7:49 frame; (d) 7:54 frame; (e) 7:59 frame; (f) 8:04 frame. (g) seismic signal recorded at the point.

4.3.2 Post-event field investigation

Field investigations and UAV surveys at Fotangba Gully began three days after the debris flow events, and local villagers confirmed that the accumulation fans had not been disturbed. UAV aerial images of the accumulation fan at the Gully mouth, along with close-ups of surface conditions, are shown in Figure 11a to c. Field measurements indicate that the fan thickness at location ① is about 1.2 m, with a thin layer (1 − 2 mm) of clay covering the surface in some areas (Figure 11c). Some rocks larger than 1 m in diameter (Figure 11b and 11c) suggest that the debris flow had a relatively high carrying capacity. Larger rocks are found at the bottom of the alluvial fan (Figure 11b), while smaller rocks are located at the front (Figure 11c), indicating that the carrying capacity of the debris flow decreases sharply after being released from the channel constraints as the cross-sectional area increases.

A sediment sample weighing about 4.7 kg was collected from the accumulation fans in Fotangba Gully to estimate the particle size distribution of the debris flow, taken from location ① in Figure 11a. Grain size analysis was performed using sieving and a Malvern particle sizer. Due to the lack of several sample analyses in this study, more analyses should be conducted for better variability estimation. We also neglected to record the portion of materials above the maximum particle size shown in the granulometric curve, which should be addressed in future research. The results indicate that clay particles (size < 0.005 mm) made up only 0.041% of the total sample weight (Figure 11d), consistent with field observations. The low cohesive sediment content in the accumulation fan sample may result from removal by post-event processes, such as the flushing action of the Minjiang River or human clearance. The particle size

https://doi.org/10.5194/egusphere-2024-2977
Preprint. Discussion started: 29 October 2024

distribution shows that 94% of the sample particles are 0.018 m, denoted as D in Eq. (6). In the next section, we will use D as a basis for analyzing the PSD curve features of the debris flow.

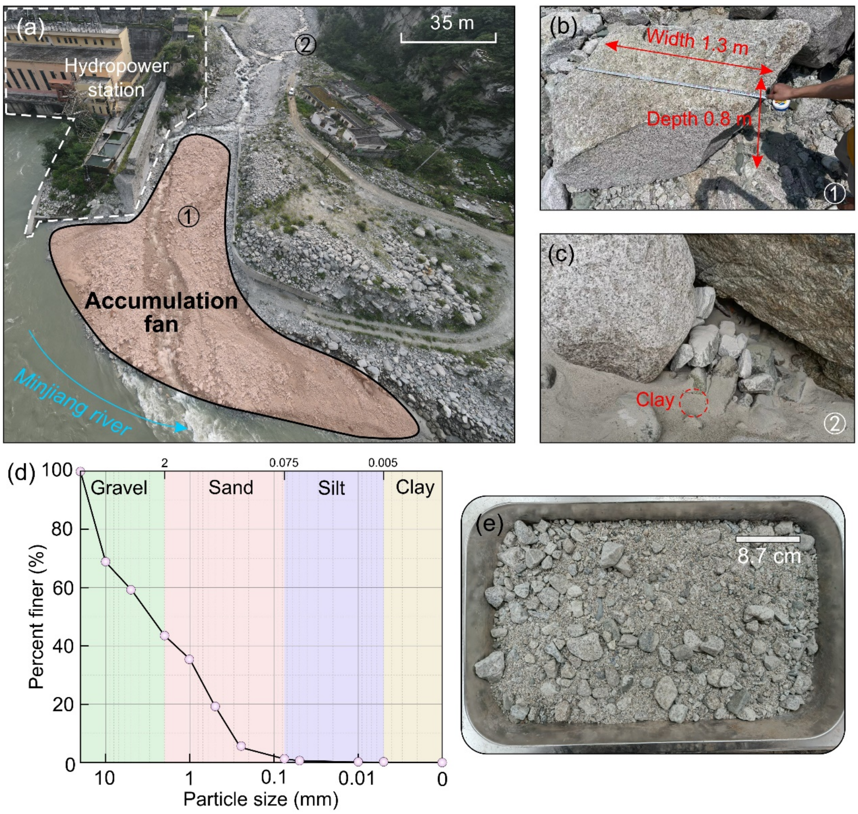

Figure 11 Post-event field survey of accumulation fans in Fotangba Gully. (a) Our aerial view of the Fotangba Gully fan; (b) Largest particle on the Fotangba Gully fan, marked ① in image (a); (c) Thin layer of clay covering the accumulation surface in Fotangba Gully, marked as ② in image (a); (d) Particle size distribution for Fotangba Gully sediment samples; (e) Fotangba Gully sediment sample. Clay has not been marked in the subplot (d) because the particles with grain size less than 0.005 mm account for 0.041% of the total weight of the sample.

https://doi.org/10.5194/egusphere-2024-2977
Preprint. Discussion started: 29 October 2024

4.3.3 PSD analysis of the key points

The seismic power spectral density (PSD) curves for six time points, corresponding to their infrared images, were calculated using Eq. (5) (Figure 12a). These curves show a clear decrease in maximum power energy from 7:39 to 8:04, with power energy initially increasing with frequency before decreasing. The maximum power energy occurs in the 20-25 Hz frequency band across all intervals. The frequency bands are categorized as low frequency (<15 Hz), main frequency (15-30 Hz), and high frequency (>30 Hz). The high-frequency power energy decreases gradually from 7:39 to 8:04, dropping rapidly from 7:39 to 7:49 and more slowly from 7:54 to 8:04. In contrast, the low-frequency power energy increases significantly from 7:39 to 7:44, sharply decreases around 7:54, and then stabilizes. These variations highlight the need for further understanding. We will use a seismic PSD forward modeling approach to interpret these results comprehensively.

We conducted debris flow seismic PSD forward modeling (Figure 12b) using Eq. (6) with parameters from observations of the second debris flow in Fotangba Gully. Particle size, D, was based on 94% of the particle size distribution, resulting in values of 0.01 m, 0.015 m, 0.02 m, and 0.025 m. Velocity, u, was set at 2 m/s, 4 m/s, and 6 m/s, consistent with the mean velocity in Section 4.2. The seismic propagation distance, r0, was measured from Point 1 to the central channel of the second debris flow. Other parameters in Eq. (6) were consistent with those used for seismic signal recovery in Section 4.1.2.

As shown in Figure 12b, debris flow velocity significantly affects the PSD energy level, while particle size has a weaker impact. For the same particle radius, energy increases sharply across the frequency band with higher flow velocities. In contrast, energy increases within specific frequency bands are modest when varying particle size at a constant flow velocity. The effect of flow velocity is more pronounced at the high-frequency end, suggesting that high-frequency energy can effectively indicate variations in flow velocity.

https://doi.org/10.5194/egusphere-2024-2977
Preprint. Discussion started: 29 October 2024

Examining the PSD curves for the six time points shows a gradual decrease at the high-frequency end, indicating a reduction in debris flow velocity. The decline is rapid from 7:39 to 7:59 and then slows down, aligning with flow rate analyses based on infrared imagery. In the low-frequency range, velocity also affects energy, but the changes are smaller than in the high-frequency range. Notably, low-frequency energy increases at 7:44 compared to 7:39, contrasting with high-frequency behavior. Figure 10c shows an infrared image indicating a higher concentration of particles in the debris flow at 7:44, suggesting that this low-frequency energy may result from these particles.

The peak frequency is influenced by both particle size and flow velocity (Figure 12b). Smaller particle sizes and higher flow velocities result in higher peak frequencies, and vice versa. This phenomenon arises from the combined effects of particle size and flow velocity. Additionally, particle content, including flux and concentration, significantly affects seismic signal energy. Therefore, when considering the model in Eq. (6), accounting for particle concentration is essential. Analyzing the peak frequency of seismic signals from 7:39 to 8:04 reveals an interesting pattern: the peak frequency increases, decreases, and then rises again. This reflects the response of particle size and flow velocity to the PSD. Specifically, as flow velocity decreases, particle size increases. Significant changes in flow velocity should correspond with changes in sediment concentration.

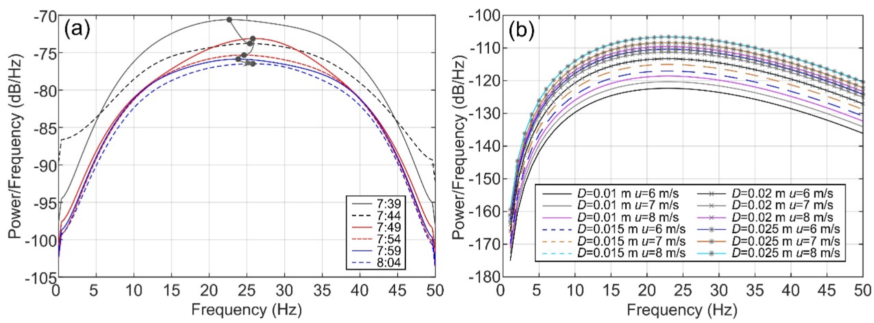

Figure 12 Characteristic change of power spectral density (PSD). (a) Evolution of PSD during the second debris flow in Fotangba Gully on the morning of August 19, 2022,

https://doi.org/10.5194/egusphere-2024-2977
Preprint. Discussion started: 29 October 2024

from 7:39 to 8:04; (b) Comparison of PSD for different grain sizes (*D*) and velocities (*u*). Each curve represents PSD frequency over 60 s. The six dots in subplot (a) correspond to the PSD maximum at the six-time points from 7:39 to 8:04, and the black arrows indicate the time course of these six-time points. The PSD values of *D*=0.015 m and *u*=8 m/s, *D*=0.02 m, and *u*=6 m/s are equal, so the curves coincide in subplot (b).

From our analysis, we conclude that in the six moments from 7:39 to 8:04, the flow velocity gradually decreases, and the particle size, particle concentration, and flow velocity first increase and then decrease. This pattern is consistent with the results of the infrared image analysis in Section 4.4.1 and confirms that the trend of the debris flow can be determined from the time-frequency characteristics of the seismic signals.

5 Discussion

5.1 Characteristics and evolution of debris flow events

The seismic signals from the three debris flow events show similar amplitude and time-frequency patterns, but variations in monitoring locations lead to differences in signal propagation and attenuation. By combining seismic signal analysis with imagery and using compensation functions to closely restore the original seismic signals, we can effectively reconstruct the debris flows' motion and dynamics. When selecting the analysis time for the Power Spectral Density (PSD) curve, it is important to consider the seismic signal characteristics and choose representative points. Estimating flow velocity and particle size is also recommended, as these factors can significantly affect the PSD curve. Integrating detailed post-disaster investigation data, dynamic parameters, and forward modeling results can greatly improve the reliability of analyzing debris flow evolution using seismic signals.

By comparing the mean velocity calculations from the cross-correlation function and Manning's formula, we observed discrepancies in the cross-correlation results for the Fotangba Gully debris flows (Table 3). Comiti et al. (2014) noted that the cross-

https://doi.org/10.5194/egusphere-2024-2977
Preprint. Discussion started: 29 October 2024

correlation function tends to underestimate debris flow velocities, a finding corroborated by this study. One potential factor influencing the velocity calculations is the distance between seismic sensors. In this study, the sensors were approximately 500 meters apart, while Arattano and Marchi (2005) suggested that sensor spacing exceeding 100 meters may reduce the accuracy of velocity calculations based on the cross-correlation function. Our velocity result of 7.0 m/s falls within the range of 3.0-9.1 m/s reported by Arattano and Marchi (2005), thereby enhancing the credibility of our findings. Additionally, the empirical nature of the Manning formula may contribute to the differences observed between the two methods (Kang, 1987). For the Er Gully debris flow, the velocity obtained through cross-correlation was an order of magnitude larger, indicating that excessively curved channels may not be suitable for velocity calculations using the cross-correlation function.

5.2 Limitations and future works

This study addresses the situation of debris flow that is difficult to reach and inconvenient to install instruments and proposes a monitoring system that is easy to monitor, reliable, and low-cost. Through this system, we can explain and analyze the debris flow process well by using seismic signal monitoring and analysis, combined with time-lapse camera image analysis, and post-event investigation. Of course, due to the unsystematic nature of the monitoring instruments (only seismic monitoring instruments and time-lapse cameras), many of the analyses in this study are mostly preliminary and lack a certain degree of accuracy. However, based on this study, we expect to improve the monitoring and analysis based on seismic signals for subsequent debris flow detection, early warning, and inversion.

There were some issues with the application of infrared cameras in the study. The cameras were not able to record images of nighttime debris flows. Even for daytime debris flows, factors such as rainfall or debris flow splashes caused water droplets to adhere to the infrared camera lens, partially blurring the recorded images. Also, the 5-minute interval between recorded images is fine for determining debris flow movement,

https://doi.org/10.5194/egusphere-2024-2977
Preprint. Discussion started: 29 October 2024

but the time resolution is too coarse to determine changes in flow characteristics during debris flow evolution. In follow-up studies, the interval between images should be decreased. It would also be useful to have a wider array of instruments at each monitoring station, including flow level gauges, to aid seismic signal analysis and velocity estimation and place more stations over a larger area to generate a larger dataset. This would allow future research to focus on the identification of early warning thresholds for debris flow disasters.

We have used the assumptions of point sources and plane waves to simplify the calculation of the compensation. Theoretically, the compensation should be calculated by integrating over the channel. However, due to variations in the response functions of the point sources at different locations in the channel and factors such as loose surface, meandering flow and varying river width, integration becomes difficult. Therefore, we chose a simplified approach. We assumed a constant propagation velocity and a constant quality factor in the propagation area, ignoring changes in river width, and calculated the weighted travel time from a river section near the monitoring point to the monitoring point itself. The compensation of the propagation effect was then based on the assumption of a plane wave. Since this method is inherently subject to some errors, we adjusted the gain factor to maximize compensation and ensure numerical stability. Accurate measurement of seismic wave propagation velocity, quality factor and flow morphology near the monitoring point would improve the accuracy of the compensation. However, these parameters are labor-intensive to measure, unstable, and significantly affected by precipitation and human subjective consciousness influences, making their repeated use difficult. Therefore, in practical applications, we integrated the line source characteristics and considered the planar features of seismic wave propagation velocity, quality factor, and river morphology near the monitoring point, adopting a numerically stable approach. This method requires careful consideration of the effects of location on the results to ensure effective and accurate compensation. In addition, there are considerable lateral fluctuations due to the weak compaction of the river channel sediments and the relative instability of these sediments. These factors increase the difficulty of compensation, which complicates the accurate measurement of the compensation parameters and reduces their reliability. In practice, we therefore adhere to the principle of numerical stability. This means that we prevent the noise energy from exceeding the signal energy and at the same time try to maximize the energy in all frequency bands.

The small dataset of the current study does not allow a broader analysis of debris flow dynamics; however, it does demonstrate the effectiveness of using an in-situ seismic network for real-time monitoring of debris flows, provides theoretical support for the inversion of debris flow dynamics, and highlights the potential for application in early warning systems.

6 Conclusions

This study successfully monitored the seismic signal characteristics of three debris flows that occurred in the Wenchuan earthquake area of China on August 19, 2022, using a near-field debris flow monitoring system. The research investigated the seismic characteristics of these three debris flows, which exhibited fast excitation and slow decay. Even after largely eliminating the propagation effect, significant differences were observed in the seismic amplitude and frequency characteristics at different monitoring stations of the same debris flow, indicating changes in the dynamic parameters of the debris flow during its evolution. By utilizing the seismic signal characteristics, the study determined the occurrence time and duration of the three debris flows and reconstructed the entire process of the second debris flow in Fotangba. Using the cross-correlation function, the average flow velocity of the second debris flow in Fotangba was determined to be 7.0 m/s, and this result was validated for reliability using the Manning formula.

In the case of Er Gully with relatively complex topography, the effectiveness of the cross-correlation function was limited, likely due to the more complex terrain

https://doi.org/10.5194/egusphere-2024-2977
Preprint. Discussion started: 29 October 2024

leading to significant variations in the kinematic parameters of the debris flow. Therefore, while the cross-correlation function may be a suitable method for calculating peak flow in simple debris flows, it may not be as appropriate for more complex debris flows.

These three debris flow events occurred under heavy rainfall conditions. Changes in the flow state of the debris flow, identified through image analysis and field investigations, resulted in different frequency ranges in the energy spectrum at the beginning and end of the debris flow, as confirmed by continuous photo analysis, PSD of current records, and forward modeling. By analyzing the seismic amplitude and frequency characteristic changes at different monitoring stations of the debris flows, rough insights into the relative changes during the evolution process of the debris flow can be obtained.

Through the case application of this study, we propose a simple, inexpensive, and remote monitoring system for the situation of debris flow monitoring stations with inconvenient installation of instruments and low budget. This study is expected to provide a theoretical basis for future debris flow monitoring and warning methods based on seismic signal and inversion methods.

Acknowledgments

This study was financially supported by the National Natural Science Foundation of China (grant nos. U21A2008, 42120104002, and 42271075), the Second Tibetan Plateau Scientific Expedition and Research Program (STEP) (grant no. 2019QZKK0906).

Code/Data availability

All raw data can be provided by the corresponding authors upon request.

https://doi.org/10.5194/egusphere-2024-2977
Preprint. Discussion started: 29 October 2024

Author contributions

The authors of this manuscript entitled "Monitoring, analysis and application of debris flow based on seismic signal" are Yan Yan, Cheng Zeng, Renhe Wang, Yifei Cui, Sheng Hu, Xinglu Wang, and Hui Tang. Yan Yan is the first author and is responsible for Conceptualization, Methodology, Writing-Original draft preparation in this research. Cheng Zeng is the second author, is responsible for data organization, validation, and revising the original draft. Renhe Wang is the third author, responsible for data collection, field investigation, and manuscript revision. Yifei Cui is the fourth author and the corresponding author, is responsible for the Review & Editing, Supervision. Sheng Hu is the fifth author and is responsible for Visualization. Xinglu Wang is responsible for the Investigation, Validation. Hui Tang is the seventh author and is responsible for Writing- Reviewing and Editing.

Competing interests

The authors declare that they have no conflict of interest.

https://doi.org/10.5194/egusphere-2024-2977
Preprint. Discussion started: 29 October 2024

References

Aaron, J., Spielmann, R., McArdell, B. W., Graf, C.: High-Frequency 3D LiDAR Measurements of a Debris Flow: A Novel Method to Investigate the Dynamics of Full-Scale Events in the Field. Geophys. Res. Lett. 50(5), e2022GL102373, https://doi.org/10.1029/2022GL102373, 2023.

Andrade, S.D., Almeida, S., Saltos, E., Pacheco, D., Hernandez, S., Acero, W.: A simple and general methodology to calibrate seismic instruments for debris flow quantification: application to Cotopaxi and Tungurahua volcanoes (Ecuador). Landslides 19(3), 747-759, https://doi.org/10.1007/s10346-021-01784-5, 2022.

Arattano, M.: On the use of seismic detectors as monitoring and warning systems for debris flows. Nat. Hazards 20(2-3), 197-213, https://doi.org/10.1023/A:1008061916445, 1999.

Arattano, M., Moia, F.: Monitoring the propagation of a debris flow along a torrent. Hydrol. Sci. J. 44(5), 811-823, https://doi.org/10.1080/02626669909492275, 1999.

Arattano, M., Marchi, L.: Measurements of debris flow velocity through cross-correlation of instrumentation data. Nat. Hazards Earth Syst. Sci. 5(1), 137-142, https://doi.org/10.5194/nhess-5-137-2005, 2005.

Arattano, M., Marchi, L.: Systems and sensors for debris-flow monitoring and warning. Sensors 8(4), 2436-2452, https://doi.org/10.3390/s8042436, 2008.

Arattano, M., Marchi, L., Cavalli, M.: Analysis of debris-flow recordings in an instrumented basin: confirmations and new findings. Natural Hazards and Earth System Sciences, 12(3), 679-686. https://doi.org/10.5194/nhess-12-679-2012, 2012.

Barrière, J., Oth, A., Hostache, R., Krein, A.: Bed load transport monitoring using seismic observations in a low-gradient rural gravel bed stream. Geophys. Res. Lett. 42(7), 2294-2301, https://doi.org/10.1002/2015GL063630, 2015.

Beason, S.R., Legg, N.T., Kenyon, T.R., Jost, R.P.: Forecasting and seismic detection of proglacial debris flows at Mount Rainier National Park, Washington, USA. Environ. Eng. Geosci. 27(1), 57-72, https://doi.org/10.2113/EEG-D-20-00014, 2021.

Belli, G., Walter, F., McArdell, B., Gheri, D., Marchetti, E.: Infrasonic and seismic analysis of debris‐flow events at Illgraben (Switzerland): Relating signal features to flow parameters and to the seismo‐acoustic source mechanism. J. Geophys. Res.-Earth Surf. 127(6), e2021JF006576, https://doi.org/10.1029/2021JF006576, 2022.

Berti, M., Genevois, R., LaHusen, R., Simoni, A., Tecca, P.R.: Debris flow monitoring in the Acquabona watershed on the Dolomites (Italian Alps). Physics and Chemistry of the Earth, Part B: Hydrology, Oceans and Atmosphere 25(9), 707-715, https://doi.org/10.1016/S1464-1909(00)00090-3, 2000.

Burtin, A., Bollinger, L., Cattin, R., Vergne, J., Nábělek, J.L.: Spatiotemporal sequence of Himalayan debris flow from analysis of high-frequency seismic noise. J. Geophys. Res. 114, F04009, https://doi.org/10.1029/2008JF001198, 2009.

Cao, C., Yu, B., Ma, E.L., Liu, S.: Study on debris flow in Fongtuba Gully after the earthquake at Wenchuan County of Sichuan Province. Journal of Sediment Research 44(1), 38-43, 2019. (in Chinese).

Chen, C.Y., Lin, L.Y., Yu, F.C., Lee, C.S., Tseng, C.C., Wang, A.H., Cheung, K.W.: Improving debris

https://doi.org/10.5194/egusphere-2024-2977
Preprint. Discussion started: 29 October 2024

flow monitoring in Taiwan by using high-resolution rainfall products from QPESUMS. Nat. Hazards 40, 447-461, https://doi.org/10.1007/s11069-006-9004-2, 2007.

Chien-Yuan, C., Tien-Chien, C., Fan-Chieh, Y., Wen-Hui, Y., Chun-Chieh, T.: Rainfall duration and debris-flow initiated studies for real-time monitoring. Environ. Geol. 47, 715-724, https://doi.org/10.1007/s00254-004-1203-0, 2005.

Comiti, F., Marchi, L., Macconi, P., Arattano, M., Bertoldi, G., Borga, M., Brardinoni, F., Cavalli, M., D'Agostino, V., Pennna, D., Theule, J.: A new monitoring station for debris flows in the European Alps: first observations in the Gadria basin. Nat. Hazards, 73, 1175-1198, https://doi.org/10.1007/s11069-014-1088-5, 2014.

Cook, K.L., Rekapalli, R., Dietze, M., Pilz, M., Cesca, S., Rao, N.P., Srinagesh, D., Paul, H., Metz, M., Mandal, P. and Suresh, G.: Detection and potential early warning of catastrophic flow events with regional seismic networks. Science, 374(6563), pp.87-92, https://doi.org/10.1126/science.abj1227, 2021.

Cook, K. L., Dietze, M.: Seismic advances in process geomorphology. Annu. Rev. Earth Planet. Sci. 50, 183-204, https://doi.org/10.1146/annurev-earth-032320-085133, 2022.

Coviello, V., Arattano, M., Turconi, L.: Detecting: torrential processes from a distance with a seismic monitoring network. Nat. Hazards 78, 2055-2080, https://doi.org/10.1007/s11069-015-1819-2, 2015.

Cui, P., Guo, X., Yan, Y., Li, Y., Ge, Y.: Real-time observation of an active debris flow watershed in the Wenchuan Earthquake area. Geomorphology 321, 153-166, https://doi.org/10.1016/j.geomorph.2018.08.024, 2018.

Cui, P., Zhou, G.G., Zhu, X.H., Zhang, J.Q.: Scale amplification of natural debris flows caused by cascading landslide dam failures. Geomorphology, 182, 173-189, https://doi.org/10.1016/j.geomorph.2012.11.009, 2013.

Dammeier, F., Moore, J.R., Hammer, C., Haslinger, F., Loew, S.: Automatic detection of alpine rockslides in continuous seismic data using hidden Markov models. J. Geophys. Res. 121(2), 351-371, https://doi.org/10.1002/2015JF003647, 2016.

Deparis, J., Jongmans, D., Cotton, F., Baillet, L., Thouvenot, F., Hantz, D.: Analysis of rock-fall and rock-fall avalanche seismograms in the French Alps. Bull. Seismol. Soc. Amer. 98(4), 1781-1796, https://doi.org/10.1785/0120070082, 2008.

Ekström, G., Stark, C.P.: Simple scaling of catastrophic landslide dynamics. Science 339(6126), 1416-1419, https://doi.org/10.1126/science.1232887, 2013.

Farin, M., Tsai, V. C., Lamb, M. P., Allstadt, K. E.: A physical model of the high-frequency seismic signal generated by debris flows. Earth Surf. Process. Landf. 44(13), 2529–2543, https://doi.org/10.1002/esp.4677, 2019.

Fuchs, F., Lenhardt, W., Bokelmann, G., AlpArray Working Group: Seismic detection of rockslides at regional scale: examples from the Eastern Alps and feasibility of kurtosis-based event location. Earth Surf. Dyn. 6(4), 955-970, https://doi.org/10.5194/esurf-6-955-2018, 2018.

Futterman, W. I.: Dispersive body waves. J. Geophys. Res. 67(13), 5279-5291, https://doi.org/10.1029/JZ067i013p05279, 1962.

Guo, N., Zhou, X., Xu, K., Wang, Y., Lyu, J, Duan, M.: Near-surface *Q*-value survey method based on uphole with hammer excitation and receiving using multi-stage geophones on wells. Oil

Geophysical Prospecting 58(2), 295-304, 2023. (in Chinese).

Guo, X., Cui, P., Li, Y., Zou, Q., Kong, Y.: The formation and development of debris flows in large watersheds after the 2008 Wenchuan Earthquake. Landslides 13, 25-37, https://doi.org/10.1007/s10346-014-0541-6, 2016.

Hibert, C., Mangeney, A., Grandjean, G., Shapiro, N.M.: Slope instabilities in Dolomieu crater, Réunion Island: From seismic signals to rockfall characteristics. J. Geophys. Res. 116, F04032, https://doi.org/10.1029/2011JF002038, 2011.

Huang, C.J., Yeh, C.H., Chen, C.Y. and Chang, S.T.: Ground vibrations and airborne sounds generated by motion of rock in a river bed. Natural Hazards and Earth System Sciences, 8(5), pp.1139-1147, https://doi.org/10.5194/nhess-8-1139-2008, 2008.

Huang, C. J., Chu, C. R., Tien, T. M., Yin, H. Y., Chen, P. S.: Calibration and deployment of a fiber-optic sensing system for monitoring debris flows. Sensors 12(5), 5835-5849, https://doi.org/10.3390/s120505835, 2012.

Huang, Z., Xu, M., Chen, W., Lin, X., Cao, C., Singh, R. P.: Postseismic restoration of the ecological environment in the Wenchuan region using satellite data. Sustainability, 10(11), 3990. https://doi.org/10.3390/su10113990, 2018.

Huang, X., Li, Z., Fan, J., Yu, D., Xu, Q.: Frequency characteristics and numerical computation of seismic records generated by a giant debris flow in Zhouqu, Western China. Pure Appl. Geophys. 177, 347-358, https://doi.org/10.1007/s00024-019-02177-5, 2020.

Hübl, J., Schimmel, A., Kogelnig, A., Suriñach, E., Vilajosana, I., McArdell, B.W.: A review on acoustic monitoring of debris flow. International Journal of Safety and Security Engineering 3(2), 105-115, https://doi.org/10.2495/SAFE-V3-N2-105-115, 2013.

Hürlimann, M., Abancó, C., Moya, J., Vilajosana, I.: Results and experiences gathered at the Rebaixader debris-flow monitoring station, Central Pyrenees, Spain. Landslides, 11, 939-953. https://doi.org/10.1007/s10346-013-0452-y, 2014.

Hürlimann, M., Coviello, V., Bel, C., Guo, X., Berti, M., Graf, C., Hürl, J., Miyata, S., Smith, J.B., Yin, H.-Y., 2019. Debris-flow monitoring and warning: Review and examples. Earth-Sci. Rev. 199, 102981, https://doi.org/10.1016/j.earscirev.2019.102981, 2014.

Hürlimann, M., Rickenmann, D., Graf, C.: Field and monitoring data of debris-flow events in the Swiss Alps. Can. Geotech. J. 40(1), 161-175, https://doi.org/10.1139/t02-087, 2003.

Iverson, R.M.: The physics of debris flows. Rev. Geophys. 35(3), 245-296, https://doi.org/10.1029/97RG00426, 1997.

Kang, Z.C.: A velocity research of debris flow and its calculating method in China. Mountain Research 5(4), 247-259, 1987.

Kean, J.W., Staley, D.M., Lancaster, J.T., Rengers, F.K., Swanson, B.J., Coe, J.A., Hernandez, J.L., Sigman, A.J., Allstadt, K.E., Lindsay, D.N.: Inundation, flow dynamics, and damage in the 9 January 2018 Montecito debris-flow event, California, USA: Opportunities and challenges for post-wildfire risk assessment. Geosphere 15(4), 1140-1163, https://doi.org/10.1130/GES02048.1, 2019.

Kean, J. W., Staley, D. M., Leeper, R. J., Schmidt, K. M., Gartner, J. E.: A low‐cost method to measure the timing of postfire flash floods and debris flows relative to rainfall. Water Resour. Res. 48(5), W05516, https://doi.org/10.1029/2011WR011460, 2012.

https://doi.org/10.5194/egusphere-2024-2977
Preprint. Discussion started: 29 October 2024

Kjartansson, E.: Constant Q‐wave propagation and attenuation. J. Geophys. Res.-Solid Earth 84(B9), 4737-4748, https://doi.org/10.1029/JB084iB09p04737, 1979.

Kogelnig, A., Hübl, J., Suriñach, E., Vilajosana, I., McArdell, B.W.: Infrasound produced by debris flow: propagation and frequency content evolution. Nat. Hazards 70, 1713-1733, https://doi.org/10.1007/s11069-011-9741-8, 2014.

Lai, V.H., Tsai, V.C., Lamb, M.P., Ulizio, T.P., Beer, A.R.: The seismic signature of debris flows: Flow mechanics and early warning at Montecito, California. Geophys. Res. Lett. 45(11), 5528-5535, https://doi.org/10.1029/2018GL077683, 2018.

Li, Z., Huang, X., Xu, Q., Yu, D., Fan, J., Qiao, X.: Dynamics of the Wulong landslide revealed by broadband seismic records. Earth, Planets and Space 69, 1-10, https://doi.org/10.1186/s40623-017-0610-x, 2017.

Liu C., Feng X., Zhang J.: A stable inverse Q filtering using the iterative filtering method. Oil Geophysical Prospecting 48(6), 890-895, 2013. (in Chinese).

Liu, S., Hu, K., Zhang, Q., Zhang, S., Hu, X., Tang, D.: Quantitative analysis of the effects of an earthquake on rainfall thresholds for triggering debris-flow events. Front. Earth Sci. 9, 676470, https://doi.org/10.3389/feart.2021.676470, 2021.

Marchetti, E., Walter, F., Barfucci, G., Genco, R., Wenner, M., Ripepe, M., McArdell, B., Price, C.: Infrasound array analysis of debris flow activity and implication for early warning. J. Geophys. Res. 124(2), 567-587, https://doi.org/10.1029/2018JF004785, 2019.

Marchi, L., Arattano, M., Deganutti, A.M.: Ten years of debris-flow monitoring in the Moscardo Torrent (Italian Alps). Geomorphology 46(1-2), 1-17, https://doi.org/10.1016/S0169-555X(01)00162-3, 2002.

McArdell, B. W., Bartelt, P., Kowalski, J.: Field observations of basal forces and fluid pore pressure in a debris flow. Geophys. Res. Lett. 34(7), L07406, https://doi.org/10.1029/2006GL029183, 2007.

McCoy, S. W., Kean, J. W., Coe, J. A., Staley, D. M., Wasklewicz, T. A., Tucker, G. E.: Evolution of a natural debris flow: In situ measurements of flow dynamics, video imagery, and terrestrial laser scanning. Geology 38(8), 735-738, https://doi.org/10.1130/G30928.1, 2010.

Moretti, L., Mangeney, A., Capdeville, Y., Stutzmann, E., Huggel, C., Schneider, D., Bouchut, F.: Numerical modeling of the Mount Steller landslide flow history and of the generated long period seismic waves. Geophys. Res. Lett. 39(16), L16402, https://doi.org/10.1029/2012GL052511, 2012.

Nagl, Georg, and Johannes Hübl. "A check-dam to measure debris flow-structure interactions in the Gadria torrent." In Advancing Culture of Living with Landslides: Volume 5 Landslides in Different Environments, Springer International Publishing, pp. 465-471. https://doi.org/10.1007/978-3-319-53483-1_55, 2017.

Rickenmann, D.: Empirical relationships for debris flows. Nat. Hazards 19, 47-77, https://doi.org/10.1023/A:1008064220727, 1999.

Roth, D. L., Brodsky, E. E., Finnegan, N. J., Rickenmann, D., Turowski, J. M., Badoux, A.: Bed load sediment transport inferred from seismic signals near a river. J. Geophys. Res.-Earth Surf. 121(4), 725-747, https://doi.org/10.1002/2015JF003782, 2016.

Schenato, L., Pasuto, A.: On the Use of Optical Fiber Sensors for Debris Flow Monitoring: A Review

https://doi.org/10.5194/egusphere-2024-2977
Preprint. Discussion started: 29 October 2024

of Recent Achievements. Belt and Road Webinar Series on Geotechnics, Energy and Environment pp. 60-70, https://doi.org/10.1007/978-981-16-9963-4_5, 2021.

Schimmel, A., Coviello, V., Comiti, F.: Debris flow velocity and volume estimations based on seismic data. Nat. Hazards Earth Syst. Sci. 22(6), 1955-1968, https://doi.org/10.5194/nhess-22-1955-2022, 2022.

Schimmel, A., Hübl, J.: Automatic detection of debris flows and debris floods based on a combination of infrasound and seismic signals. Landslides 13, 1181-1196, https://doi.org/10.1007/s10346-015-0640-z, 2016.

Schneider, D., Bartelt, P., Caplan‐Auerbach, J., Christen, M., Huggel, C., McArdell, B.W.: Insights into rock-ice avalanche dynamics by combined analysis of seismic recordings and a numerical avalanche model. J. Geophys. Res. 115, F04026, https://doi.org/10.1029/2010JF001734, 2010.

Strick, E.: The determination of Q, dynamic viscosity and transient creep curves from wave propagation measurements. Geophys. J. Int. 13(1-3), 197-218, https://doi.org/10.1111/j.1365-246X.1967.tb02154.x, 1967.

Suwa, H., Okano, K., Kanno, T.: Behavior of debris flows monitored on test slopes of Kamikamihorizawa Creek, Mount Yakedake, Japan. International Journal of Erosion Control Engineering 2(2), 33-45, https://doi.org/10.13101/ijece.2.33, 2009.

Tang, C., Rengers, N.V., Van Asch, T.W., Yang, Y.H., Wang, G.F.: Triggering conditions and depositional characteristics of a disastrous debris flow event in Zhouqu city, Gansu Province, northwestern China. Nat. Hazards Earth Syst. Sci. 11(11), 2903-2912, https://doi.org/10.5194/nhess-11-2903-2011, 2011.

Tecca, P.R., Galgaro, A., Genevois, R., Deganutti, A.M.: Development of a remotely controlled debris flow monitoring system in the Dolomites (Acquabona, Italy). Hydrol. Process. 17(9), 1771-1784, https://doi.org/10.1002/hyp.1212, 2003.

Tsai, V.C., Minchew, B., Lamb, M.P., Ampuero, J.P.: A physical model for seismic noise generation from sediment transport in rivers. Geophys. Res. Lett. 39(2), L02404, https://doi.org/10.1029/2011GL050255, 2012.

Van Herwijnen, A., Schweizer, J.: Monitoring avalanche activity using a seismic sensor. Cold Reg. Sci. Tech. 69(2-3), 165-176, https://doi.org/10.1016/j.coldregions.2011.06.008, 2011.

Vilajosana, I., Suriñach, E., Abellán, A., Khazaradze, G., Garcia, D., Llosa, J.: Rockfall induced seismic signals: case study in Montserrat, Catalonia. Nat. Hazards Earth Syst. Sci. 8(4), 805-812, https://doi.org/10.5194/nhess-8-805-2008, 2008.

Walter, F., Burtin, A., McArdell, B.W., Hovius, N., Weder, B., Turowski, J.M.: Testing seismic amplitude source location for fast debris-flow detection at Illgraben, Switzerland. Nat. Hazards Earth Syst. Sci. 17(6), 939-955, https://doi.org/10.5194/nhess-17-939-2017, 2017.

Xu, M.D., Feng, Q.H.: Roughness of debris flows. Proceeding of the First Conference of Chinese Research of Debris Flows, pp. 51-52, 1979. (in Chinese).

Yan, Y., Cui, P., Chen, S., Chen, X., Chen, H., Chien, Y.: Characteristics and interpretation of the seismic signal of a field-scale landslide dam failure experiment. J. Mt. Sci. 14, 219-236, https://doi.org/10.1007/s11629-016-4103-3, 2017.

Yang, W., Wang, X., Yi, H., et al.: Research and Application of Near-Surface Structure Investigation Techniques in the Loess Plateau Region of the Ordos Basin. In: Proceedings of the 2019

https://doi.org/10.5194/egusphere-2024-2977
Preprint. Discussion started: 29 October 2024

Petroleum Exploration Technology Symposium. China Petroleum Society, Petroleum Geophysical Exploration Committee, Chinese Geophysical Society, Exploration Geophysics Committee. Changqing Geophysical Prospecting Division, BGP Inc., China National Petroleum Corporation, pp. 4, 2019. (in Chinese).

Yan, Y., Cui, Y., Huang, X., Zhou, J., Zhang, W., Yin, S., Guo, J., Hu, S.: Combining seismic signal dynamic inversion and numerical modeling improves landslide process reconstruction. Earth Surf. Dynam. 10, 1233–1252, https://doi.org/10.5194/esurf-10-1233-2022, 2022.

Yan, Y., Cui, Y., Liu, D., Tang, H., Li, Y., Tian, X., Zhang, L., Hu, S.: Seismic signal characteristics and interpretation of the 2020 "6.17" Danba landslide dam failure hazard chain process. Landslides 18, 2175-2192, https://doi.org/10.1007/s10346-021-01657-x, 2021.

Yan, Y., Tang, H., Hu, K., Turowski, J. M., Wei, F.: Deriving debris-flow dynamics from real-time impact-force measurements. J. Geophys. Res. 128, e2022JF006715, https://doi.org/10.1029/2022JF006715, 2023.

Yan, Y., Cui, Y., Tian, X., Hu, S., Guo, J., Wang, Z., Yin S., Liao, L.: Seismic signal recognition and interpretation of the 2019 "7.23" Shuicheng landslide by seismogram stations. Landslides 17, 1191-1206, https://doi.org/10.1007/s10346-020-01358-x, 2020.

Yu, G., Lim, S.Y.: Modified Manning formula for flow in alluvial channels with sand-beds. J. Hydraul. Res. 41(6), 597-608, https://doi.org/10.1080/00221680309506892, 2003.

Zhang, Z., Walter, F., McArdell, B. W., Haas, T., Wenner, M., Chmiel, M., He, S.: Analyzing bulk flow characteristics of debris flows using their high frequency seismic signature. J. Geophys. Res.-Solid Earth 126(12), e2021JB022755, https://doi.org/10.1029/2021JB022755, 2021.

Zhang, Z.: Study on the inversion of dynamic parameters of landslides and debris flows based on seismic signals. University of Chinese Academy of Sciences, 2021. (in Chinese).